Journal of Colloid and Interface Science 524 (2018) 368–378

Contents lists available at ScienceDirect

Journal of Colloid and Interface Science

journal homepage: www.elsevier.com/locate/jcis

Regular Article

High-response and low-temperature nitrogen dioxide gas sensor based on gold-loaded mesoporous indium trioxide

Shan Li [a], Ming Cheng [a], Guannan Liu [a], Lianjing Zhao [a], Bo Zhang [a], Yuan Gao [a,*], Huiying Lu [a], Haiyu Wang [a], Jing Zhao [b], Fangmeng Liu [a], Xu Yan [a], Tong Zhang [a], Geyu Lu [a,*]

[a] State Key Laboratory on Integrated Optoelectronics, Jilin Province Key Laboratory on Advanced Gas Sensors, College of Electronic Science and Engineering, Jilin University, 2699 Qianjin Street, Changchun 130012, China
[b] College of Electrical and Electronic Engineering, Changchun University of Technology, 2055 Yanan Street, Changchun 130012, China

GRAPHICAL ABSTRACT

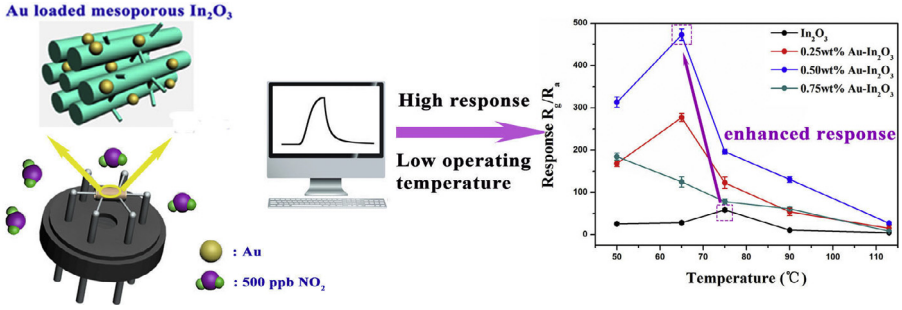

ARTICLE INFO

Article history:
Received 1 February 2018
Revised 8 April 2018
Accepted 9 April 2018
Available online 10 April 2018

Keywords:
NO_2
Gas sensor
Mesoporous material
Au
In_2O_3

ABSTRACT

Nitrogen dioxide (NO_2), as a typical threatening atmospheric pollutant, is hazardous to the environment and human health. Thus, the development of a gas sensor with high response and low detection limit for NO_2 detection is highly important. The highly ordered mesoporous indium trioxide (In_2O_3) prepared by simple nanocasting method using mesoporous silica as template and decorated with Au nanoparticles was investigated for NO_2 detection. The prepared materials were characterized by X-ray diffraction, transmission electron microscopy, and X-ray photoelectron spectroscopy. Characterization results showed that the samples exhibited ordered mesostructure and were successfully decorated with Au. The gas sensing performance of the sensors based on a series of Au-loaded mesoporous In_2O_3 were systematically investigated. The Au loading level strongly affected the sensing performance toward NO_2. The optimal sensor, which was based on 0.5 wt% Au-loaded In_2O_3, displayed high sensor response and low detection limit of 10 ppb at low operating temperature of 65 °C. The excellent sensing properties were mainly attributed to the ordered mesoporous structure and the catalytic performance of Au. We believe that the Au-loaded mesoporous In_2O_3 can provide a promising platform for NO_2 gas sensors with excellent performance.

1. Introduction

NO_2 is mainly produced in industrial emissions and automobile exhaust. This gas is one of the main environmental pollutants and the leading cause of acid rain and photochemical smog [1–5].

* Corresponding authors.
E-mail addresses: gaoyuan@jlu.edu.cn (Y. Gao), lugy@jlu.edu.cn (G. Lu).

https://doi.org/10.1016/j.jcis.2018.04.033
0021-9797/

NO_2 is not only detrimental to the environment but also has hazardous effects on human health even at extremely low concentration. In fact, people will feel physical discomfort when exposed to 15 ppb of NO_2 [6]. Moreover, continuous exposure to even 53 ppb NO_2 may cause damage to the respiratory system, especially serious for children [7]. Therefore, the development of the NO_2 sensor with high response and low detection limit is imperative.

Many gas sensors based on semiconductor oxides have been reported to monitor NO_2. Several popular sensitive materials are SnO_2, ZnO, WO_3, and In_2O_3 [8–11]. These NO_2 gas sensors usually have good response at a high working temperature (≥100 °C), which can provide adequate thermal energy for the reaction or desorption of gas molecules. However, the high operating temperature may cause high power consumption and several safety issues in practical application. In addition, carbon-based materials or hybrids have been implemented to reduce operating temperature because of the good electronic conductivity and carrier mobility of carbon, but their inherent relative low response should be further improved [12,13]. Consequently, high response detection of NO_2 at operating temperature below 100 °C is still a challenge.

The morphology, chemical composition, and structure of the semiconductor metal-oxide material are the main factors that affect the sensitive properties of gas sensors. Compared with other nanostructures, mesoporous metal oxides have large specific surface area and porous structure with pore size of 2–50 nm. These features can favor the diffusion of the target gas in their pore channels and simultaneously provide a large number of surface active sites for the host–guest interactions [14–19]. In particular, Zhang et al. synthesized WO_3 mesoporous hollow nanospheres doped with Fe and achieved a wide detection range for NO_2 detection at 120 °C [5]. Wang et al. successfully prepared mesoporous and ultrathin In_2O_3 nanosheets, which exhibited excellent gas sensing performance toward NO_x gas. The response of the sensor reached 213 toward 10 ppm NO_x under a relatively low operating temperature (120 °C) [20]. In addition, loading noble metals on metal oxide was confirmed to be effective in enhancing the sensitivity and reducing the operating temperature. Sui et al. decorated MoO_3 hollow spheres with Au and effectively improved the sensitivity of gas sensor for benzene, toluene, and xylene detection. Their optimum working temperature decreased by 40 °C compared with pure MoO_3 hollow spheres [21]. Fu et al. enhanced the sensing performance by adding Au nanoparticles (NPs) on rod-like In_2O_3 in detecting CO at room temperature. However, pure In_2O_3 had no response to CO at the same conditions [22]. Ying et al. synthesized mesoporous WO_3 with 0.5 wt.% Ag using three-dimensional cubic KIT-6 as a hard template. The response was 44 for 1 ppm NO_2 at 75 °C [15]. However, the effect of Au decoration on the NO_2 sensing properties of mesoporous In_2O_3 is rarely reported.

In this paper, we prepared mesoporous In_2O_3 with SBA-15 mesoporous silica as a template by simple nanocasting method and then employed Au as catalyst to decorate mesoporous In_2O_3 to improve the sensor response and further reduce the operating temperature. The nanostructural and componential information of the prepared ordered mesoporous materials were characterized, and their sensing properties were investigated in detail.

2. Experimental

2.1. Preparation of mesoporous materials

$In(NO_3)_3{\cdot}4.5H_2O$ (≥99.5%), ethanol (≥99.9%), and sodium hydroxide (≥96%) were purchased from Beijing Chemical industry. Hydrogen tetrachloroaurate (III) trihydrate ($HAuCl_4{\cdot}3H_2O$, ≥99.9%) was purchased from Sigma Aldrich. All reagents were used as received without further purification. The water used in all experiments had a resistivity higher than 18.2 MΩ·cm.

Highly ordered two-dimensional mesoporous SBA-15, one kind of the most common mesoporous silica with a hexagonal array of pores, was synthesized according to a method described elsewhere [18]. Mesoporous In_2O_3 was prepared with the nanocasting method using mesoporous silica SBA-15 as a template. The detailed synthesis procedure is given below. Typically, 1.72 g of $In(NO_3)_3{\cdot}4.5H_2O$ was dissolved in 10 ml of ethanol and continuously stirred to form a homogeneous solution. Then, 0.5 g of SBA-15 was added into the precursor solution, which was stirred at 40 °C, until all ethanol had totally evaporated. The obtained precipitate was calcined at 300 °C for 3 h. This process was repeated twice with the dosage of metal salts reduced by half at each time to fully impregnate the template. At the last calcined treatment, the products were calcined at 500 °C for 3 h. During several times of calcined treatments, the indium nitrate decomposed to synthesize indium oxide. The excess NaOH (2 mol/L) solution was used to etch the silica template. The etching process was repeated thrice. Finally, the mesoporous In_2O_3 was obtained.

A series of Au-loaded mesoporous In_2O_3 materials (Au-In_2O_3) with different Au mass ratios (0.25 wt%, 0.5 wt%, and 0.75 wt%) were prepared using an established impregnation method [19]. $HAuCl_4$ with different weight percentages to In_2O_3 (0.5 wt%, 1.0 wt%, and 1.5 wt%) were added into and mixed uniformly with the mesoporous In_2O_3 (0.1 g) dispersion in 10 ml of ethanol. The dispersion was continuously stirred at 40 °C, until ethanol evaporated completely. After calcination at 300 °C for 2 h, the corresponding products were obtained and marked as S1, S2, S3, and S4. During the calcined process, hydrogen tetrachloroaurate decomposed to synthesize Au.

2.2. Characterization

The X-ray diffraction (XRD) pattern was carried out by a Rigaku D/Max-2550 diffractometer employing Cu-Kα radiation (λ = 1.54178 Å). Thermogravimetric analysis (TG, Netzsch, STA449 F3 jupiter) was used to testify the thermal behaviors of the mesoporous materials. The heating rate was 10 °C/min in air from 50 °C to 900 °C. Nitrogen adsorption isotherm was recorded with a Micromeritics Gemini VII apparatus and the samples were degassed under vacuum at 77 K for 22 h. Brunauer-Emmett-Teller (BJT) equation was used to estimate the specific surface area. The pore size distribution was performed on the Barrett-Joyner-Halenda method. The scanning electron microscopy (SEM) images were recorded on JEOL JSM-7500F microscope operating at 15 kV. The images of Transmission electron microscopy (TEM), high-resolution transmission electron microscopy (HRTEM) and element distribution analysis were obtained by using a JEOL JEM-2100 microscope operated. The substrate that supports detected materials is the carbon-coated Cu grid. X-ray photoelectron spectroscopy (XPS) measurements were recorded on a Thermo ESCALAB 250 spectrometer. The adventitious carbon C 1s peak at 284.8 eV was used as the reference for calibration the binding energy.

2.3. Fabrication and measurement of gas sensor

The schematics of the fabricated gas sensor and sensor static testing system are shown in Fig. 1. The as-obtained powder materials were mixed with some deionized water to form a paste. Then, the homogeneous paste was coated onto the external surface of an alumina ceramic tube. The ceramic tube had a pair of Au electrodes with Pt lead wires, which connected to the measuring system. After the sensing devices were sintered at 400 °C for 2 h, a Ni-Cr alloy coil as a heater was inserted into the ceramic tube to control

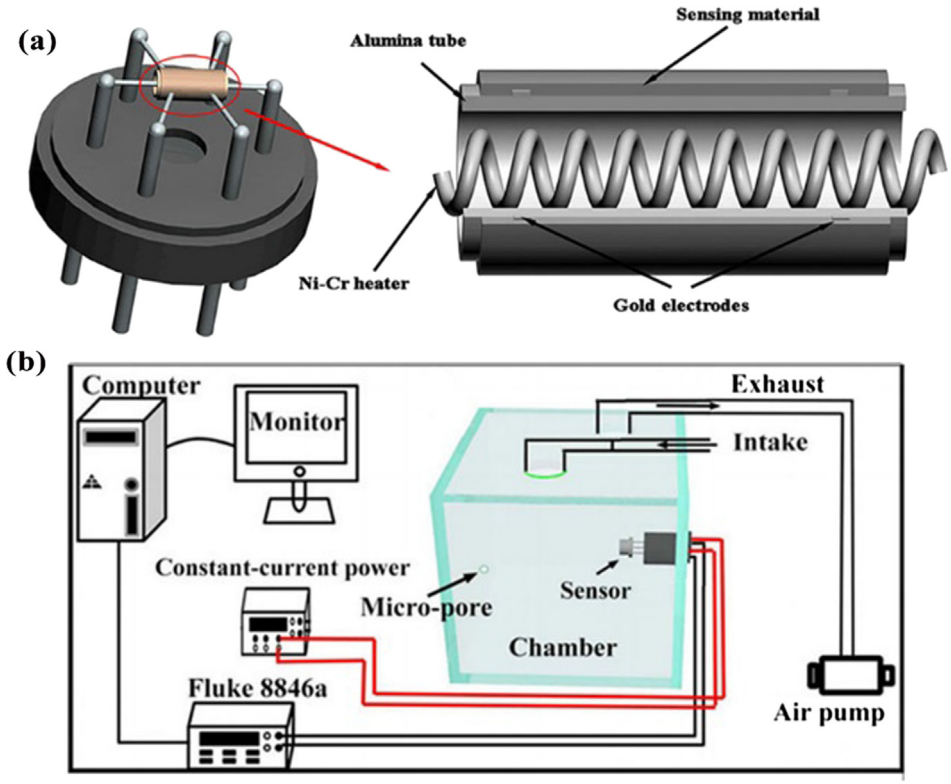

Fig. 1. (a) Schematic structure of the gas sensor; (b) Schematic illustration of sensor static testing system.

the operating temperature. The gas sensing properties were measured as follows. The sensor was put into the chamber, and a given amount of the tested gas was injected into the chamber. After obtaining a stable response, the test gas was removed and replaced by air using an air pump. The real-time resistances of the device were recorded using a digital multimeter (Fluke 8846A). The test data were displayed on a computer. The operating temperature was controlled by adjusting the constant-current power. The sensor response was defined as Response = R_a/R_g (reducing gas) and Response = R_g/R_a (oxidizing gas). R_a means the sensor resistance in air while R_g is the resistance in the target gas. The response and recovery time were defined as the time taken to achieve 90% of the total resistance change after the sensor to expose to the tested gas and air case, respectively.

3. Results and discussion

3.1. Material characterization

X-ray diffraction patterns were recorded to investigate the long-range order of pores and the crystal structure of the samples. The low-angle XRD patterns of all samples are shown in Fig. 2(a). Each pattern of the mesoporous materials exhibited a sharp strong diffraction peak that can be indexed to (1 0 0) and two unobtrusively weak peaks corresponding to (1 1 0) and (2 2 0). These results matched well with the XRD patterns of SBA-15 in the literature [18,23]. Thus, the as-made samples had successfully replicated mesoporous structure from the SBA-15 template. However, the diffraction peaks of these replicas had lower intensity compared with that of SBA-15. This phenomenon indicated that the mesoporous structure of the samples was partially destroyed, although a certain order remained [23]. The wide-angle XRD patterns of S1–S4 are shown in Fig. 2(b). All diffraction peaks of In_2O_3 presented a good match with the typical cubic structure of In_2O_3 (JCPDS card 06-0416). No obvious diffraction peaks were attributable to Au in S2–S4 probably because of the low amount of Au loaded in the mesoporous In_2O_3 or the homogenous distribution of Au particles [15]. The thermogravimetric (TG) analysis of the materials was investigated as shown in Fig. S1 (see supplementary information).

The morphologies of samples were further investigated by SEM and TEM. The SEM images of S1 and S3 were provided in the Fig. S2 (see supplementary information), which shows fiber-like aggregates of mesoporous nanostructure. Fig. 3(a) and (b) present the TEM images of S1 and S3. The obtained materials showed a highly ordered pore structure before and after modification by Au particles, and the measured pore widths of S1 and S3 were approximately 3.5 nm and 3.2 nm, respectively. Fig. 3(b) and (c) illustrate the mesoporous structure with several Au particles. The mean diameters of Au were 26.1 nm and 28.8 nm in S3 (Fig. 3b) and S4 (Fig. 3c), respectively. Comparative results illustrated that the size of Au NPs decorated on the mesoporous In_2O_3 slightly increased with increase in Au dosage. This phenomenon supported the hypothesis that Au tends to nucleate and aggregate during deposition. The HRTEM image in Fig. 3(d) clearly illustrates that the region involved a single Au particle and presents two different lattice fringes spacing of 0.29 nm and 0.23 nm which corresponded to the (2 2 2) planes of In_2O_3 and (1 1 1) planes of Au, respectively. To clarify the distribution of Au in the sample, elemental mapping analysis of S3 [Fig. 3(b)] was performed, and the results are shown in Fig. 4a–c. Elements In and O exhibited high density as the main components of the sample. In Fig. 4(c), some Au particles were dispersed uniformly in the mesoporous In_2O_3 and others aggregated on the surface of the sample. Earlier studies by Jiang et al. showed that the interaction energies of Ag, Pt, or Pd deposited on α-Fe_2O_3 were much higher with a porous/rough surface than with a smooth one [24,25] Similarly, Au deposited on In_2O_3 surface needed lower total potential energy of the Au particles. Hence, Au particles tended to aggregate and grow on the surface of mesopores rather than be entirely dispersed into mesoporous In_2O_3.

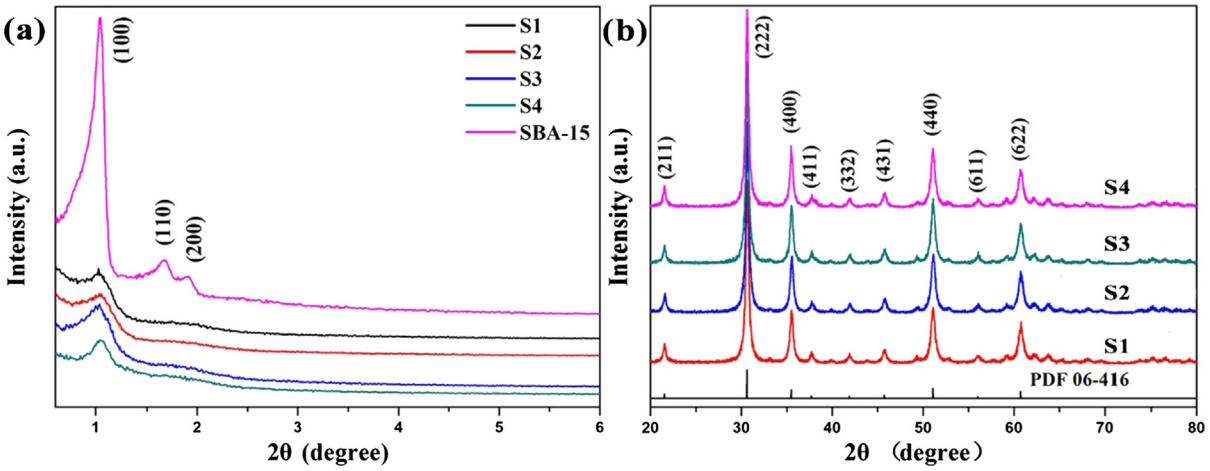

Fig. 2. (a) Low-angle XRD patterns of all mesoporous materials (b) XRD patterns of S1–S4.

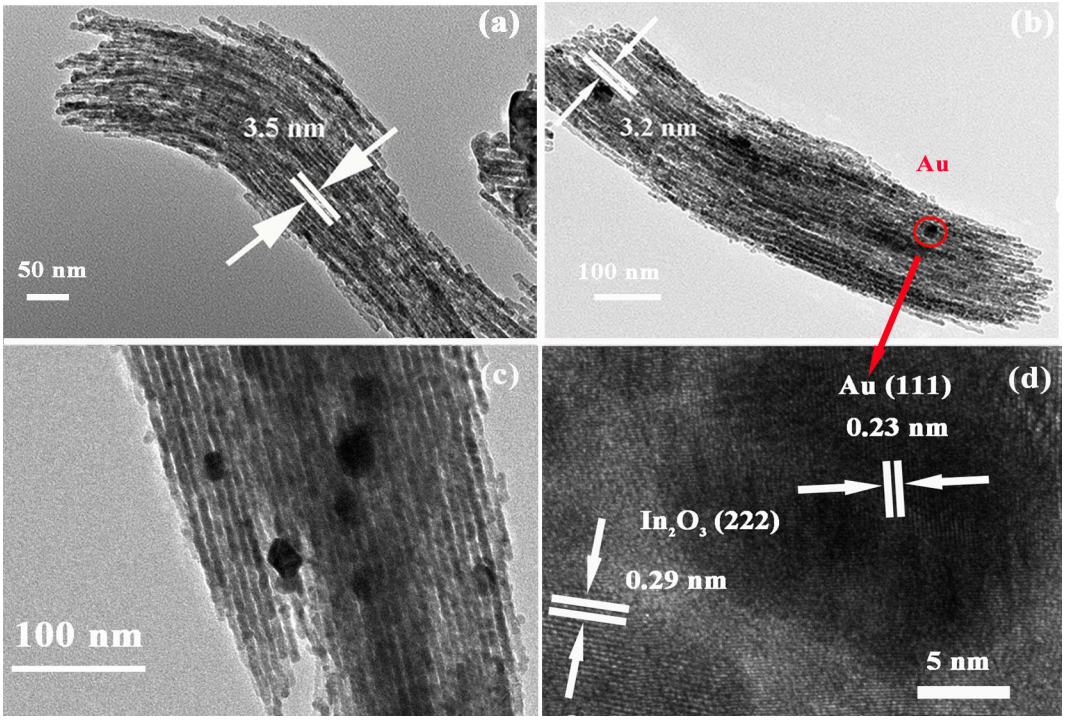

Fig. 3. TEM images of S1 sample (a), TEM images of S3 sample (b), TEM images of S4 sample (c), HRTEM image of the selected area of S3 sample (d).

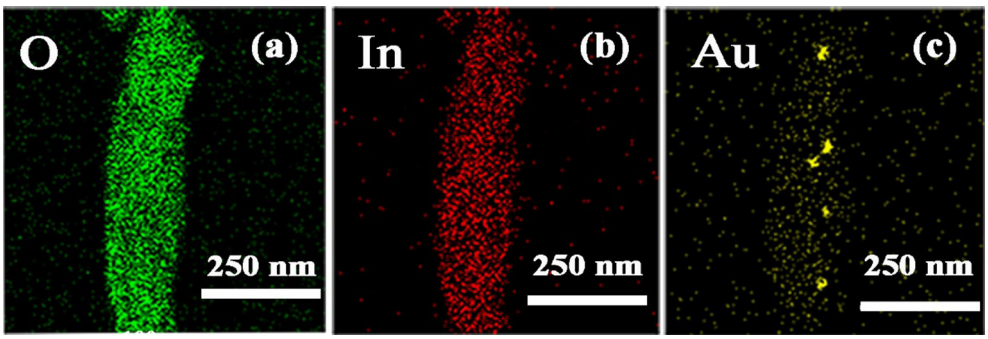

Fig. 4. Elemental mapping of mesoporous S3 sample (b): distribution of O elemental (a), In elemental (b), and Au elemental (c).

The nitrogen adsorption/desorption isotherms and pore size distribution curves of all composites are shown in Fig. 5. All curves show typical IV type isotherm, indicating the mesoporous structures of all prepared materials. The pore size distribution is shown in the insets, which illustrated one sharp peak at approximately 3.8 nm in each inset. The specific surface area, pore size, and pore volume of the samples are summarized in Table 1. The mesoporous materials had large surface areas in the range of 42.3–48.9 m^2/g. Particularly, Au-In_2O_3 (S2–S3) possessed larger specific surface and higher pore volume than pure In_2O_3 (S1) probably because the incorporated Au adhered onto the In_2O_3 skeleton, which affected the integrity and mesoporous structure [19]. However, increasing the Au load resulted in a slight decrease in the surface area and reduced pore width. This phenomenon is probably due to the blocking of the pores and formation of larger Au NPs because of the increased Au particles [26].

To obtain more information on the chemical states of surface composition, the as-synthesized S1–S4 were further characterized by X-ray photoelectron spectroscopy. Fig. 6(a) shows that the spectra of the surface composition mainly consisted of In and O elements. The spectrum in Fig. 6(b) shows two significant binding energy peaks at 83.2 eV and 86.9 eV corresponding to the electronic states of Au $4f_{7/2}$ and Au $4f_{5/2}$. According to the literature, binding energies of 84 eV and 87.7 eV belonged to the spin-orbit splitting component of Au $4f_{7/2}$ level in metallic Au, confirming that the Au element was in a single metallic state [27]. The binding energy of Au showed a negative shift of 0.8 eV compared with bulk Au, which is probably due to the strong electronic interaction between Au NPs and In_2O_3 [28]. The intensity of the peak was evidently enhanced by increasing the Au content [Fig. 6(c)]. The real loading results of Au in S3 and S4 are calculated as 0.44 wt%, 0.79 wt% from XPS spectra. We did not detect Au from XPS spectra of S2 because its concentration in S2 might be lower than the lowest detect limitation of the instrument.

Table 1
The textural properties of the mesostructured material.

Sample	Surface area (m^2/g)	Pore size (nm)	Pore volume (cm^3/g)
S1	42.32	3.84	0.12
S2	48.87	3.81	0.13
S3	46.74	3.77	0.13
S4	45.45	3.74	0.13

The high-resolution X-ray photoelectron spectra of O 1s of S1 and S3 are shown in Fig. 6(d) and (e). The spectrum of O 1s could be resolved to two Gaussian function peaks with energies of 529.7 eV and 531.5 eV. The peak at 529.7 eV could be assigned to the lattice oxygen, while that at 531.5 eV was due to the existence of adsorbed oxygen species [29]. The surface-absorbed oxygen species play a significant role in gas sensing, because they can react with the detected gas [30]. We estimated the O_{ads} percentage of two as-prepared samples and found that O_{ads} percentage of S3 was superior to that of S1. Given the intensive interaction of electronic with oxygen with the Au particle on the surface, the content of O_{ads} in Au-In_2O_3 samples were obviously superior to that before decoration.

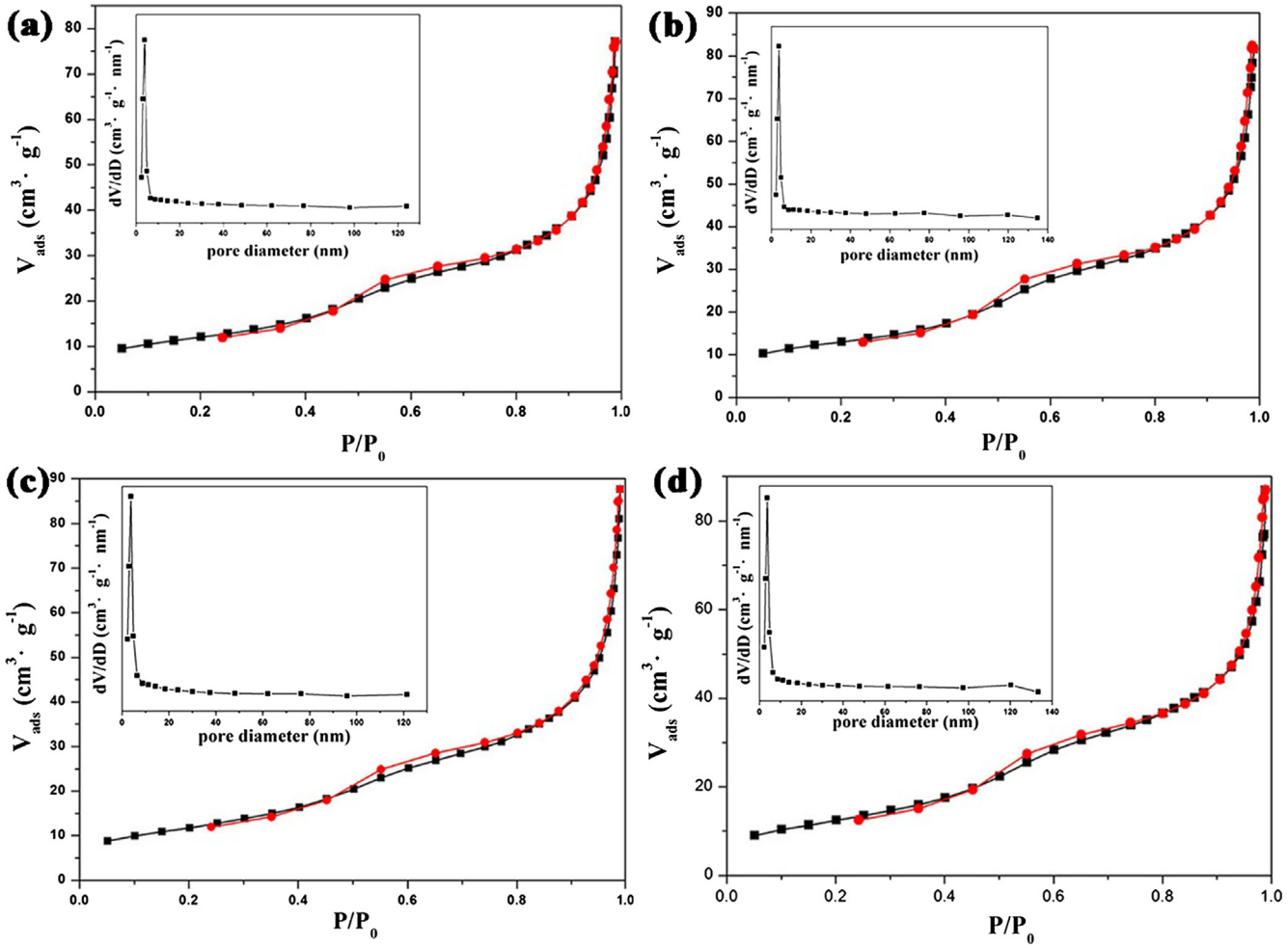

Fig. 5. Nitrogen adsorption/desorption isotherms and the pore size distributions of S1 sample (a), S2 sample (b), S3 sample (c), S4 sample (d).

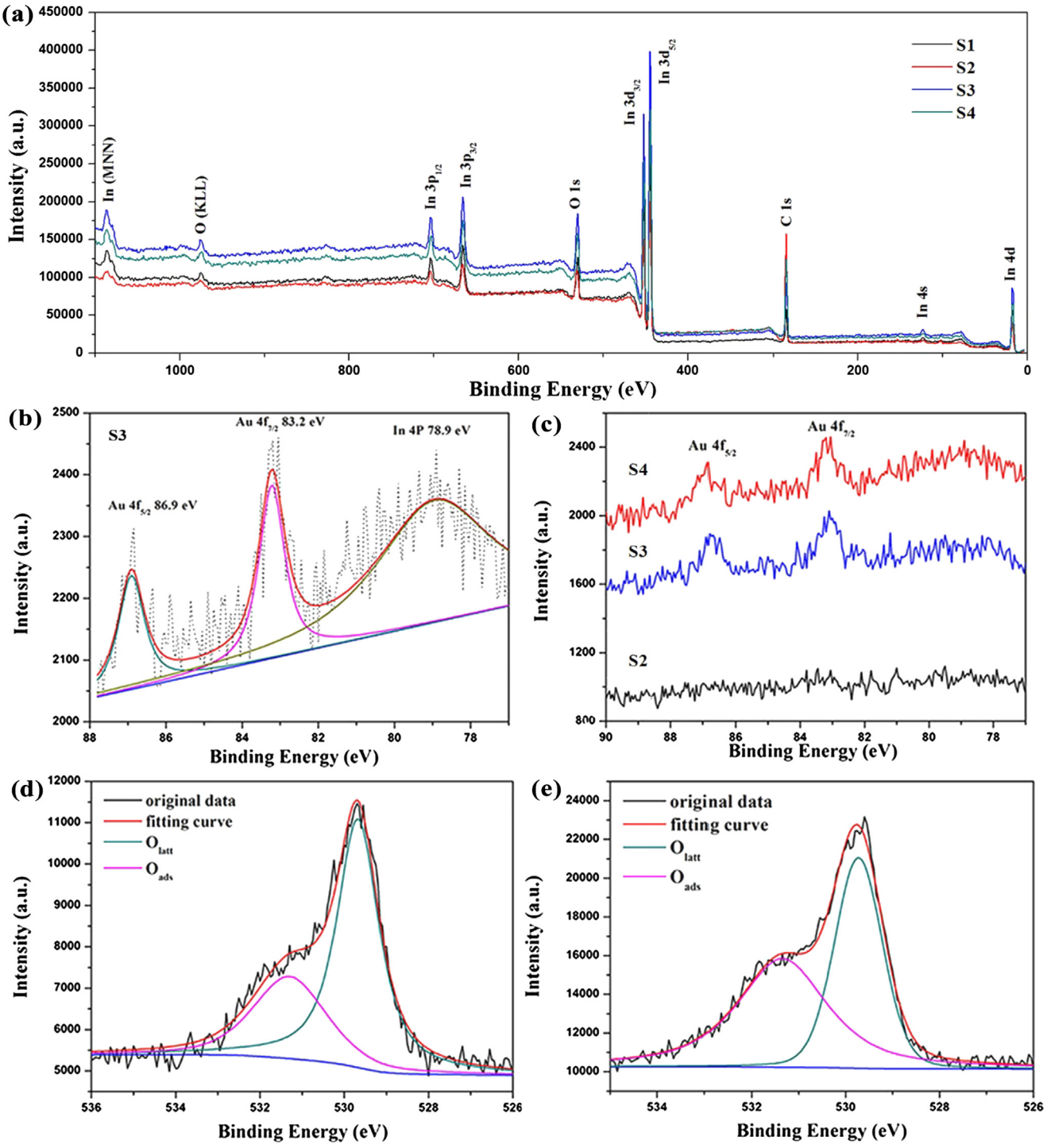

Fig. 6. (a) XPS spectra of the obtained materials, (b) Au spectrum of S3 sample, (c) Au spectrum of S2-S4 samples, (d) O 1s spectrum of S1 sample, (e) O 1s spectrum of S3 sample.

3.2. Sensing properties

To explore the effect of Au loading on the mesoporous In_2O_3 on the gas sensor performance, we evaluated the sensing properties of a series of prepared gas sensors. We first investigated the operating temperature, which is important to determine the sensor performance. Fig. 7 presents the response of the S1–S4 gas sensors to 500 ppb NO_2 within the operating temperature range of 50–115 °C. Except for the curve of the S4 sensor, most curves first rose to maximum values and then fell as the temperature increased. The response of S4 at temperature below 50 °C cannot be detected because of its overloaded resistance to 500 ppb NO_2. The low responses at low temperature were responsible for the insufficient thermal energy for NO_2 molecules to overcome the activation energy barrier of the surface reaction. As the temperature increased, adequate thermal energy obtained contributed greatly to the increased sensitivity. Then, the response was reduced beyond the optimum operating temperature, because gas adsorption was inhibited at high temperature [31–33]. The response of S1 gas sensor to 500 ppb NO_2 was much lower than the responses

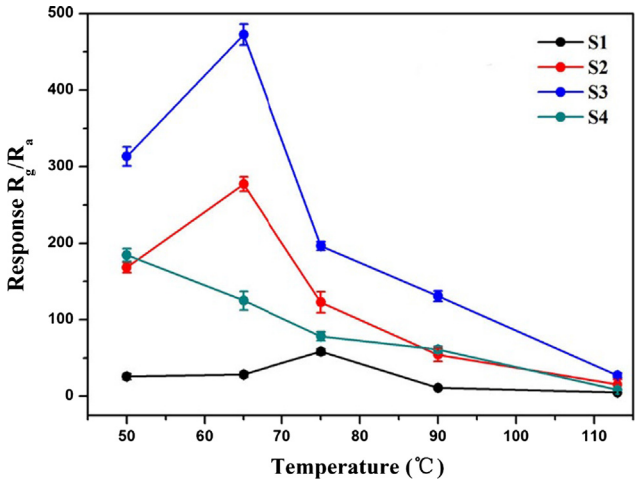

Fig. 7. The response of sensors based on S1–S4 towards 500 ppb of NO_2 as a function of operating temperature. The error bars were estimated by three measurements.

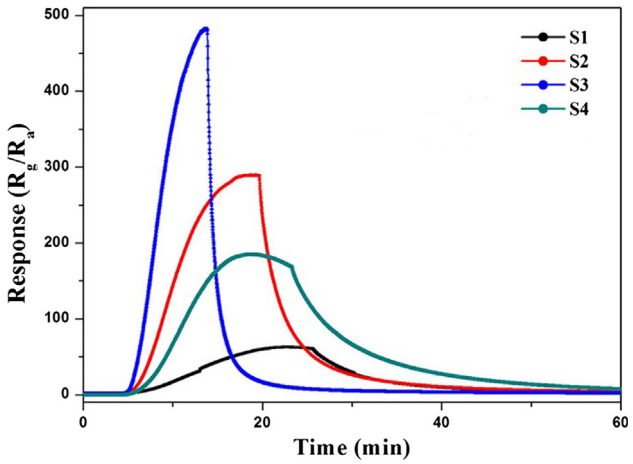

Fig. 9. The response-recovery curves of the all samples to 500 ppb NO_2 at their optimum operating temperature.

of the other sensors, with maximum value of 66.5 at 75 °C, while the responses of the S2, S3, and S4 gas sensors were 277.1 at 65 °C, 472.4 at 65 °C, and 184.5 at 50 °C, respectively. The latter sensors had obvious corresponding sensor response enhancement of 4.2, 7.1, and 2.8 times that of S1. Moreover, the optimum operating temperature displayed a decreasing tendency with increase in Au load. This result was due to the fact that addition of Au effectively reduced the activation energy. The S4 gas sensor had the lowest optimum operating temperature, but its response was inferior to S2 and S3 samples.

Gas responses to different NO_2 concentrations at specific optimal operating temperatures of the gas sensors were investigated, and the results are shown in Fig. 8. The response of the S1 gas sensor showed the lowest value toward different concentrations of NO_2 among materials. The results indicated that introducing Au NPs had a great effect on improving the sensing performance of the sensor based on mesoporous In_2O_3. The detection limit of the S3 gas sensor even reached 10 ppb NO_2, with response of 2.28 [Fig. 8(b)]. However, when the loading amount of Au was over 0.5 wt%, the response of the gas sensor decreased probably because of the reduced interfacial sites between Au and mesoporous In_2O_3 and decreased catalytic efficiency of Au. These phenomena are the consequences of the overloading of Au [19].

The response and recovery characteristics are also important parameters of gas sensor for detecting NO_2 at low temperature. Moreover, low temperature detection generally indicates the sacrificing response or recovery speed [31]. As shown in Fig. 9, the time of response and recovery of the S2–S4 gas sensors to 500 ppb NO_2 were obviously shorter than those of the S1 sensor at their respective optimal operating temperatures. Especially, the response and recovery times of the S3 sensor were much lower than the others. The results demonstrated that S3 contributed to the optimal Au catalytic activity to improve NO_2 sensing properties.

Hence, 0.5 wt% Au was considered as the optimum loading amount for NO_2 gas sensor. Fig. 10(a) shows the dynamic response and recovery curve of S3 sensor in the range of NO_2 concentrations from 10 ppb to 1 ppm at its optimum operating temperature of 65 °C. In addition, the response did not appear to level off in the tested concentration range, indicating that the sensor possessed a wide concentration range of NO_2 detection with upper limit of over 1 ppm. Fig. 10(b) displays the logarithmic plots of the sensing response ($S = R_g/R_a$) and NO_2 concentration (C, ppm). The response of the S3 sensor showed a nearly linear relationship ($R^2 = 0.971$) to NO_2 concentration in the range of 10 ppb–1 ppm. The sensing properties (working temperature, response to a certain NO_2 concentration, and detection limit) of several NO_2 sensors are

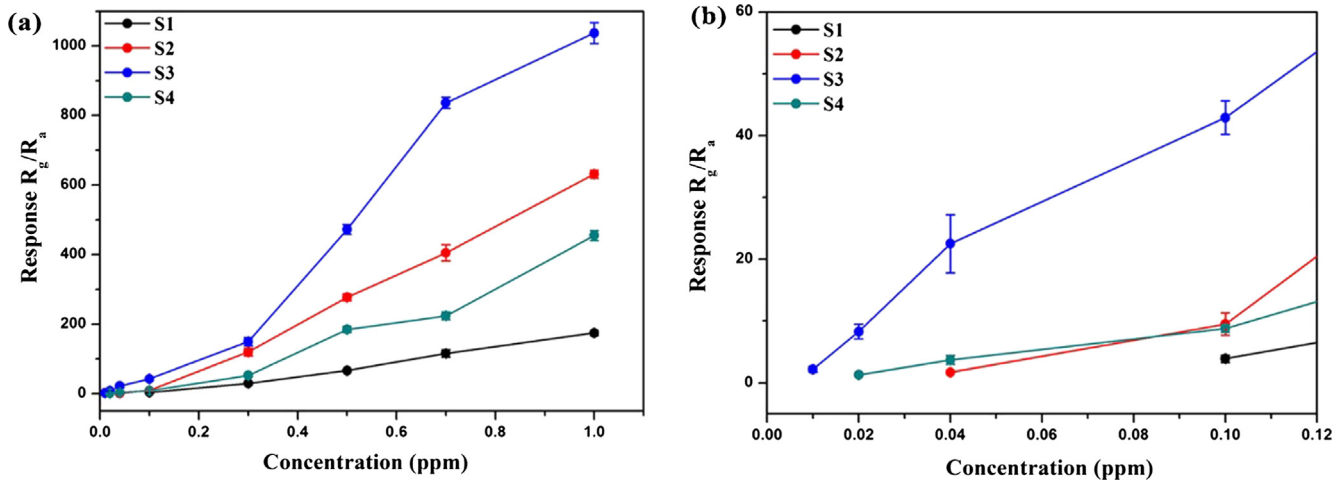

Fig. 8. (a) The response of sensors based on mesoporous samples to different concentration NO_2 at each optimum operating temperature, (b) The magnification of sensor response in the NO_2 concentration range of 10 ppb–100 ppb. The error bars were estimated by three measurements.

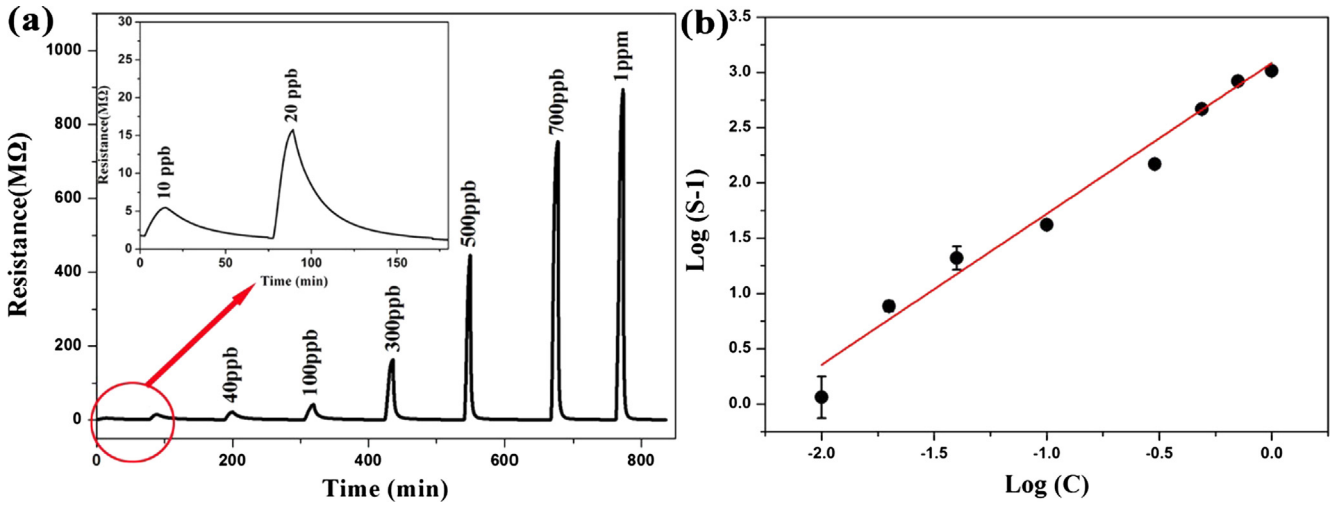

Fig. 10. (a) The dynamic response curve of the S3 sensor to 500 ppb NO_2 at optimum operating temperature, (b) Calibration curves for the S3 sensor.

compared in Table 2. The S3 sensor was evidently superior in sensor response, working temperature, and detection limit.

We also studied the selectivity of S3 sensor towards various gases, such as NH_3, Cl_2, CH_4, H_2S, CO, SO_2, and O_3 and volatile organic compounds (VOCs). The results are shown in Fig. 11(a), which revealed that the response of the S3 sensor was the highest even toward lower concentration of NO_2 compared with other ppm-level concentrations of the target gas. Almost no response to VOCs, such as ethanol, acetone, and benzene, was observed, demonstrating the excellent selectivity of the S3 sensor to NO_2. This phenomenon may be caused by the excellent sensitivity of In_2O_3 material for oxidizing gases, such as NO_2 and O_3, at low temperature [34]. Although the sensor exhibited an obvious response to O_3 at the same concentration as NO_2, the response to NO_2 was still superior by 10-fold. Moreover, the sensor response was recorded for the coexisting gases of 500 ppb NO_2 with other high-concentration interfering gases, such as NH_3, CH_4, Cl_2, SO_2, CO, and O_3. The results are shown in Fig. 11(b). The sensor response

Table 2
Comparison of the sensing performances of various mesoporous metal-oxide sensors for NO_2.

Material	Operating temperature	NO_2 concentration	Response	Detection limit	Ref.
Mesoporous WO_3 nanoparticles	200 °C	500 ppb	50.7	200 ppb	[42]
Fe doped mesoporous WO_3	120 °C	500 ppb	2.7	10 ppb	[5]
Ag-loaded mesoporous WO_3	75 °C	1 ppm	44	100 ppb	[15]
mesoporous ZnO@Au microspheres	250 °C	1 ppm	10.71	500 ppb	[43]
In_2O_3 decorated mesoporous NiO	Room temperature	15 ppm	3	5 ppm	[44]
In_2O_3 Microspheres	80 °C	500 ppb	320	50 ppb	[45]
Porous corundum In_2O_3 nanosheet	250 °C	50 ppm	164	1 ppm	[46]
Mesoporous In_2O_3	150 °C	250 ppb	10.5	50 ppb	[47]
Au loaded mesoporous In_2O_3	65 °C	500 ppb	472.4	10 ppb	This work

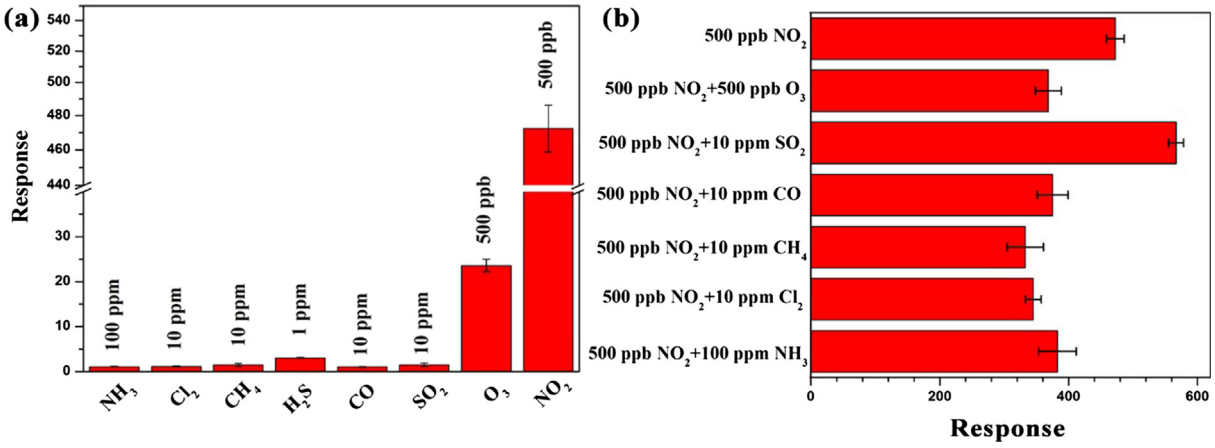

Fig. 11. (a) The sensitivity of the S3 sensor toward various gases at 65 °C, (b) Response of the S3 sensor toward various coexisting gases at 65 °C.

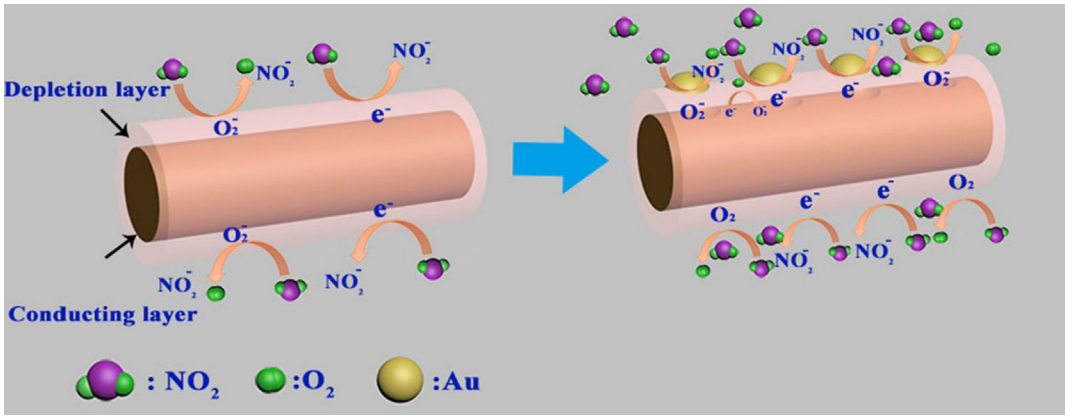

Fig. 12. Schematic illustration of the gas-sensing mechanism of the sensors towards NO_2.

to coexisting gases varied in the range of 70.4–120% compared with that to individual 500 ppb NO_2. This result demonstrated that the S3 sensor had good selectivity to NO_2. Consequently, the results clearly showed that the S3 sensor has superior selectivity to NO_2 among other gases at the same conditions.

3.3. Gas sensing mechanism

The sensing mechanism of oxide semiconductors is widely considered as follows. When the sensors are exposed to gas, the resistance of the sensing materials is changed because of the chemical adsorption and the reaction of the gas on the surface of the sensing materials [35]. In_2O_3 is a typical *n*-type metal oxide semiconductor whose conductivity mainly due to the concentration of free electrons. The gas-sensing mechanism of the sensors is illustrated in Fig. 12. When mesoporous In_2O_3 is placed in the air, some oxygen molecules are adsorbed on the mesoporous surface, and capture free electrons from the conduction band of In_2O_3 material to form chemisorbed oxygen species (O_2^-, O^-, or O^{2-}). The decrease in the concentration of free electrons further creates electronic depletion layer on the In_2O_3 surface. When the operating temperature is below 150 °C, the oxygen species primarily exist in the form of O_2^-. Once the sensor is placed under a NO_2 environment, NO_2 will move to the interface and not only capture the electron from conduction band of In_2O_3 but also combine with O_2^- as the following equation [36,37].

$$NO_2 + e^- \rightarrow NO_2^- \quad (1)$$

$$NO_2 + O_2^- \rightarrow NO_2^- + O_2 \quad (2)$$

More electrons travel from the conduction band of In_2O_3 to the interface, and the depletion width is further increased, resulting in an increase in resistance.

The excellent sensing performance of sensors based on Au-loaded mesoporous In_2O_3 can be attributed to the following aspects. First, the merits of mesoporous nanostructure of materials with well-ordered porous structures and high specific surface area contributed to enhance the sensitivity [15]. The well-ordered porous structures with connected pathway are conducive to gas diffusion. The high specific surface area with numerous active sites facilitates the gas-semiconductor interaction. Second, the decoration of Au further improves the NO_2 sensor performance. Chemical and electronic sensitization effects are the main reasons for the role of Au in improving the NO_2 sensing properties [24,38], As a chemical sensitizing agent, Au particles, as effective oxygen dissociation catalyst, could reduce the reaction activation energy and expedite the diffusion of adsorbed oxygen to the surface vacancies to yield oxygen ions. The quantity of the adsorbed oxygen and the conversion rate of the oxygen ions cloud increased in the presence of Au on the surface [39]. The other factor was electronic sensitization. Because of the work function difference between Au (5.1 eV) and In_2O_3 (4.8 eV), a Schottky junction was formed between the Au and In_2O_3, and electron transferred from In_2O_3 to Au. This phenomenon resulted in the extended electron depletion on the In_2O_3 surface and enhancement in NO_2 response [40,41]. However, the specific surface area between a series of Au-In_2O_3 showed slight decreasing trend, because the increasing content of Au particles blocked the pores and formed larger Au NPs. Hence, although the surface area is one of the important factors that determine the sensing performance, it is speculated that the catalysis of Au particle is the determining factor for the enhancement of the sensing response of Au-In_2O_3. Nonetheless, overloading of Au may cause a wide range of agglomeration to larger particles and the diminishing of active sites at the interfaces, leading to weakened Au catalytic efficiency. This even eventually resulted in the recession in sensing properties [19,48]. Consequently, the sensor based on 0.5 wt% Au loaded In_2O_3 exhibited the highest sensitivity among all fabricated sensors.

4. Conclusions

In summary, periodically ordered mesoporous Au-loaded In_2O_3 were successfully prepared via a simple hard-template method followed by an impregnation process. The low-angle XRD patterns and TEM images demonstrated the ordered mesoporous nanostructure of samples. The elemental mapping analysis and XPS results confirmed the distribution and content of Au. The sensing properties of the gas sensors based on mesoporous In_2O_3 and Au-In_2O_3 samples were investigated. The results indicated that the sensors based on Au-In_2O_3 exhibited higher response than pure In_2O_3. Among the series of Au-In_2O_3 samples, 0.5 wt% Au-In_2O_3 is optimal for NO_2 sensor with the highest response at low operating temperature of 65 °C, which sensor response enhanced 7.1 times than that of pure In_2O_3 towards 500 ppb NO_2. The linear calculation curve of 0.5 wt% Au-In_2O_3 were established in the NO_2 concentration range of 10 ppb–1 ppm, and the detection limit of 10 ppb was realized. These excellent properties can be attributed to the unique mesoporous structure and the catalytic effect of Au nanoparticles. The modification strategy of Au-loading effectively enhanced the sensor response and reduced detection limit. Thus, mesoporous In_2O_3 with optimized Au decorations is a highly promising candidate for NO_2 sensor with high response, low detection limit, and excellent selectivity at low operating temperature.

Acknowledgements

This work was supported by the National Nature Science Foundation of China (61304242, 61520106003, 61603059), National High-Tech Research and Development Program of China (863 Program, No. 2014AA06A505), Science and Technology Development Program of Jilin Province (Nos. 20150520091JH, 20160520088JH).

Appendix A. Supplementary material

Supplementary data associated with this article can be found, in the online version, at https://doi.org/10.1016/j.jcis.2018.04.033.

References

[1] A. Ruiz, G. Sakai, A. Cornet, K. Shimanoe, J. Ramon, Cr-doped TiO_2 gas sensor for exhaust NO_2 monitoring, Sens. Actuat. B: Chem. 93 (2003) 509–518.
[2] G. Lu, N. Miura, N. Yamazoe, Stabilized zirconia-based sensors using WO_3 electrode for detection of NO or NO_2, Sens. Actuat. B: Chem. 65 (2000) 125–127.
[3] P. Sekhar, E. Brosha, R. Mukundan, W. Li, M. Nelson, P. Palanisamy, F. Garzon, Application of commercial automotive sensor manufacturing methods for NO_x/NH_3 mixed potential sensors for on-board emissions control, Sens. Actuat. B: Chem. 144 (2010) 112–119.
[4] D. Perner, U. Platt, Detection of nitrous acid in the atmosphere by differential optical absorption, Geophys. Res. Lett. 6 (1979) 917–920.
[5] Z. Zhang, M. Haq, Z. Wen, Z. Ye, L. Zhu, Ultrasensitive ppb-level NO_2 gas sensor based on WO_3 hollow nanospheres doped with Fe, Appl. Surf. Sci. 434 (2018) 891–897.
[6] E. Tseliou, V. Bessa, G. Hillas, V. Delimpoura, G. Papadaki, C. Roussos, S. Papiris, P. Bakakos, S. Loukides, Exhaled nitric oxide and exhaled breath condensate pH in severe refractory asthma, CHEST J. 138 (2010) 107–113.
[7] D. Zhang, Z. Liu, C. Li, T. Tang, X. Liu, S. Han, B. Lei, C. Zhou, Detection of NO_2 down to ppb levels using individual and multiple In_2O_3 nanowire devices, Nano Lett. 4 (2010) 1919–1924.
[8] T. Kida, A. Nishiyama, Z. Hua, K. Suematsu, M. Yuasa, K. Shimanoe, WO_3 nano lamella gas sensor: porosity control using SnO_2 nanoparticles for enhanced NO_2 sensing, Langmuir 30 (2013) 2571–2579.
[9] S. Ingole, S. Navale, Y. Navale, D. Bandgar, F. Stadler, R. Mane, N. Ramgir, S. Gupta, D. Aswal, V. Patil, Nanostructured tin oxide films: physical synthesis, characterization, and gas sensing properties, J. Colloid Interface Sci. 493 (2017) 162–170.
[10] S.W. Choi, S.H. Jung, S.S. Kim, Significant enhancement of the NO_2 sensing capability in networked SnO_2 nanowires by Au nanoparticles synthesized via γ-ray radiolysis, J. Hazard. Mater. 665 (2016) 173–179.
[11] J. Hua, Y. Liang, Y. Sun, Z. Zhao, M. Zhang, P. Li, W. Zhang, Y. Chen, S. Zhuiykov, Highly sensitive NO_2 detection on ppb level by devices based on Pd-loaded In_2O_3 hierarchical microstructures, Sens. Actuat. B: Chem. 252 (2017) 116–126.
[12] Z. Wang, C. Zhao, T. Han, Y. Zhang, S. Liu, T. Fei, G. Lu, T. Zhang, High-performance reduced graphene oxide-based room-temperature NO_2 sensors: a combined surface modification of SnO_2 nanoparticles and nitrogen doping approach, Sens. Actuat. B: Chem. 242 (2017) 269–279.
[13] S. Cui, Z. Wen, E. Mattson, S. Mao, J. Chang, M. Weinert, C. Hirschmugl, M. Gajdardziska-Josifovsk, J. Chen, Indium-doped SnO_2 nanoparticle-graphene nanohybrids: simple one-pot synthesis and their selective detection of NO_2, J. Mater. Chem. 1 (2013) 4462–4467.
[14] A. Stanoiu, S. Somacescu, J. Maria, C. Moreno, V. Teodorescu, O. Florea, A. Sackmann, C. Simion, Low level NO_2 detection under humid background and associated sensing mechanism for mesoporous SnO_2, Sens. Actuat. B: Chem. 231 (2016) 166–174.
[15] Y. Wang, X. Cui, Q. Yang, J. Liu, Y. Gao, P. Sun, G. Lu, Preparation of Ag-loaded mesoporous WO_3 and its enhanced NO_2 sensing performance, Sens. Actuat. B: Chem. 225 (2016) 544–552.
[16] J. Gao, H. Wu, J. Zhou, L. Yao, G. Zhang, S. Xu, Y. Xie, L. Li, K. Shi, Mesoporous In_2O_3 nanocrystals: synthesis, characterization and NO_x gas sensor at room temperature, New J. Chem. 40 (2016) 1306–1311.
[17] T. Wagner, S. Haffer, C. Weinberger, D. Klaus, M. Tiemann, Mesoporous materials as gas sensors, Chem. Soc. Rev 42 (2013) 4036–4053.
[18] J. Zhao, W. Wang, Y. Liu, et al., Ordered mesoporous Pd/SnO2 synthesized by a nanocasting route for high hydrogen sensing performance, Sens. Actuat. B: Chem. 160 (2011) 604–608.
[19] Y. Wang, B. Zhang, J. Liu, Q. Yang, et al., Au-loaded mesoporous WO3: preparation and n-butanol sensing performances, Sens. Actuat. B: Chem. 236 (2016) 67–76.
[20] X. Wang, J. Su, H. Chen, G. Li, Z. Shi, H. Zou, X. Zou, Ultrathin In_2O_3 nanosheets with uniform mesopores for highly sensitive nitric oxide detection, ACS Appl. Mater. Interfaces 9 (2017) 16335–16342.
[21] L. Sui, X. Zhang, X. Cheng, P. Wang, Y. Xu, S. Gao, Au-loaded hierarchical MoO_3 hollow spheres with enhanced gas-sensing performance for the detection of BTX (benzene, toluene, and xylene) and the sensing mechanism, ACS Appl. Mater. Interfaces 9 (2017) 1661–1670.
[22] H. Fu, C. Hou, F. Gu, D. Han, Z. Wang, Facile preparation of rod-like Au/In_2O_3 nanocomposites exhibiting high response to CO at room temperature, Sens. Actuat. B: Chem. 243 (2017) 516–524.
[23] T. Waitz, T. Wagner, T. Sauerwald, C.D. Kohl, M. Tiemann, Ordered mesoporous In_2O_3: synthesis by structure replication and application as a methane gas sensor, Adv. Funct. Mater. 19 (2009) 653–661.
[24] J. Yue, X. Jiang, A. Yu, Molecular dynamics study on metal-deposited iron oxide nanostructures and their gas adsorption behavior, J. Phys. Chem. C 116 (2012) 8145–8153.
[25] Y. Kaneti, Q. Zakaria, Z. Zhang, C. Chen, J. Yue, M. Liu, X. Jiang, A. Yu, Solvothermal synthesis of ZnO-decorated α-Fe_2O_3 nanorods with highly enhanced gas-sensing performance toward n-butanol, J. Mater. Chem. 2 (2014) 13283–13292.
[26] Q. Hao, Y. Zhao, H. Yang, Z. Liu, Z. Liu, Alumina grafted to SBA-15 in supercritical CO_2 as a support of cobalt for fischer-tropsch synthesis, Energy Fuels 26 (2012) 6567–6575.
[27] P. Sangpour, O. Akhavan, A. Moshfegh, M. Roozbehi, Formation of gold nanoparticles in heat-treated reactive co-sputtered Au–SiO_2 thin films, Appl. Surf. Sci. 254 (2007) 286–290.
[28] Mashkoor, Y. Shi, N. Amjad, H. Sun, W. Shen, M. Wei, Synthesis of hierarchical flower-like ZnO nanostructures and their functionalization by Au nanoparticles for improved photocatalytic and high-performance li-ion battery anodes, J. Mater. Chem. 21 (2011) 7723–7729.
[29] J. Dupin, D. Gonbeau, P. Vinatier, A. Levasseur, Systematic XPS studies of metal oxides, hydroxides and peroxides, Phys. Chem. 2 (2000) 1319–1324.
[30] D. Andreeva, T. Tabakova, V. Idakiev, P. Christov, R. Giovanoli, Au/α-Fe_2O_3 catalyst for water-gas shift reaction prepared by preposition-precipitation, Appl. Catal. A 169 (1998) 9–14.
[31] C. Wang, L. Guo, N. Xie, X. Kou, Y. Sun, X. Chuai, S. Zhang, H. Song, Y. Wang, G. Lu, Enhanced nitrogen oxide sensing performance based on tin-doped tungsten oxide nanoplates by a hydrothermal method, J. Colloid Interface Sci. 512 (2018) 740–749.
[32] G. Neri, A. Bonavita, G. Micali, G. Rizzo, E. Callone, G. Carturan, Resistive CO gas sensors based on In_2O_3 and $InSnO_x$ nanopowders synthesized via starch-aided sol-gel process for automotive applications, Sens. Actuat. B 132 (2008) 224–233.
[33] X. Zhou, W. Feng, C. Wang, X.L. Hu, X.W. Li, P. Sun, K. Shimanoe, N. Yamazoe, G. Y. Lu, Porous ZnO/$ZnCo_2O_4$ hollow spheres: synthesis, characterization, and applications in gas sensing, J. Mater. Chem. A 2 (2014) 17383–17690.
[34] S. Roso, D. Degler, E. Llobet, N. Barsan, A. Urakawa, Temperature-dependent NO_2 sensing mechanisms over indium oxide, ACS Sens. 2 (2017) 1272–1277.
[35] X. Li, J. Liu, H. Guo, X. Zhou, C. Wang, P. Sun, X. Hu, G. Lu, Au@In2O3 core-shell composites: a metal-semiconductor heterostructure for gas sensing applications, RSC Adv. 5 (2015) 545–551.
[36] J. Zhao, T.L. Yang, Y.P. Liu, Z.Y. Wang, X.W. Li, Y.F. Sun, Y. Du, Y.C. Li, G.Y. Lu, Enhancement of NO_2 gas sensing response based on ordered mesoporous Fe-doped In_2O_3, Sens. Actuat. B: Chem. 191 (2014) 806–812.
[37] C. Zhang, A. Boudiba, P.D. Marco, R. Snyders, M. Ovilier, M. Debliquy, Room temperature responses of visible-light illuminated WO_3 sensors to NO_2 in sub-ppm range, Sens. Actuat. B: Chem. 181 (2013) 395–401.
[38] Y. Shim, L. Zhang, D. Kim, Y. Choi, S. Nahm, C. Kang, W. Lee, H. Jang, Highly sensitive and selective H_2 and NO_2 gas sensors based on surface-decorated WO_3 nanoigloos, Sens. Actuat. B: Chem. 198 (2014) 294–301.
[39] L. Wang, H. Dou, Z. Lou, T. Zhang, Encapsuled nanoreactors (Au@SnO_2): a new sensing material for chemical sensor, Nanoscale 5 (2013) 2686–2691.
[40] D.A. Egger, E. Zojer, Anticorrelation between the evolution of molecular dipole moments and induced work function modifications, J. Phys. Chem. Lett. 4 (2013) 3521–3526.
[41] C. Su, H. Lin, Direct toute to tungsten oxide nanorod bundles: micro-structures and electro-optical properties, J. Phys. Chem. C 113 (2009) 4042–4046.
[42] E. Heidari, C. Zamani, E. Marzbanrad, B. Raissi, S. Nazarpour, WO_3-based NO_2 sensors fabricated through low frequency AC electrophoretic deposition, Sens. Actuat. B: Chem. 146 (2010) 165–170.
[43] S. Navale, C. Liu, Z. Yang, V. Patil, P. Cao, B. Du, R. Mane, F. Stadler, Low-temperature wet chemical synthesis strategy of In_2O_3 for selective detection of NO_2 down to ppb levels, J. Alloy. Compd. 735 (2018) 2102–2110.
[44] Z. Dong, S. Liu, In_2O_3-decorated ordered mesoporous NiO for enhanced NO_2 sensing at room temperature, J. Mater. Sci. 29 (2018) 292645–292653.
[45] X. Hu, X. Zhou, B. Wang, P. Sun, X. Li, Chen Wang, J. Liu, G. Lu, Facile synthesis of hollow In_2O_3 microspheres and their gas sensing performances, RSC Adv. 5 (2015) 4609–4614.
[46] L. Gao, Z. Cheng, Q. Xiang, Y. Zhang, J. Xu, Porous corundum-type In_2O_3 nanosheets: synthesis and NO_2 sensing properties, Sens. Actuat. B: Chem. 208 (2015) 436–443.
[47] Y. Ren, X. Zhou, W. Luo, P. Xu, Y. Zhu, X. Li, X. Cheng, Y. Deng, D. Zhao, Amphiphilic block copolymer templated synthesis of mesoporous indium oxides with nanosheet-assembled Pore Walls, Chem. Mater. 28 (2016) 7997–8005.
[48] S. Kabcum, N. Kotchasak, D. Channeic, A. Tuantranontd, A. Wisitsoraatd, S. Phanichphante, C. Liewhirana, Highly sensitive and selective NO_2 sensor based on Au-impregnated WO_3 nanorods, Sens. Actuat. B: Chem. 252 (2017) 523–536.

Shan Li is presently studying the MS degree in the Electronics Science and Engineering department, Jilin University. Her research directions involve fabrication of mesoporous oxide semiconductor and their applications in gas sensors.

Ming Cheng received his BE degree from Jilin University of China in 2017. He is currently working toward the MS degree in the Electronics Science and Engineering department, Jilin University. His current researches focus on the preparation and application of graphene and semiconductor oxide, especially in gas sensor.

Guannan Liu received his BE degree from Jilin University of China in 2015. He is currently working toward the MS degree in the Electronics Science and Engineering department, Jilin University. His current research is focus on the synthesis of carbon dots and their applications.

Lianjing Zhao received her M.S. degree in 2013 from Jilin University, China. She is currently studying for her Ph.D. degree in College of Electronic Science and Engineering, Jilin University. Her research interests mainly focus on the development of the functional nanomaterials and their applications in chem/biosensor.

Bo Zhang received the BE degree in College of Chemistry from Jilin University in 2013. He is currently working toward the Dr. degree in College of Electronic Science and Engineering, Jilin University. His research interests include the synthesis of graphene and its applications in gas sensors.

Yuan Gao received her PhD degree from Department of Analytical Chemistry at Jilin University in 2012. Now she is an associate professor in Jilin University, China. Her current research is focus on the preparation and application of graphene and semiconductor oxide, especial in gas sensor and biosensor.

Huiying Lu received his MS degree from College of Chemistry, Jilin University, China in 2012 and received his PhD degree from College of Chemistry, Jilin University, China in 2015. He is currently studying for his post-doctoral degree in College of Electronic Science and Engineering, Jilin University, China.

Haiyu Wang received the PhD degree in Changchun institute of optics, fine mechanics and physics, Chinese academy of science in 2000. Now he is a professor of Jilin University, China. Now, he is interested in the studying of ultrafast laser spectroscopy.

Jing Zhao received her Doctor's degree in College of Electronic Science and Engineering from Jilin University, China, in 2013. Presently, she is a lecturer in Changchun University of Technology, China. Her current research is the application of gas sensors and humidity sensors.

Fangmeng Liu received his B.S. degree in 2009 from College of Chemistry, Liaocheng University and M.S. degree in 2012 from Northeast Forestry University in China. Currently he is studying for his Ph.D. degree in College of Electronic Science and Engineering, Jilin University, China.

Xu Yan received his M.S degree in 2013 from Nanjing Agricultural University. He joined the group of Prof. Xingguang Su at Jilin University and received his Ph.D. degree in June 2017. Since then, he did postdoctoral work with Prof. Geyu Lu and Prof. Junqiu Liu. Currently, his research interests mainly focus on the development of the functional nanomaterials for chem/bio sensors.

Tong Zhang completed her MS degree in semiconductor materials in 1992 and her PhD in the field of microelectronics and solid-state electronics in 2001 from Jilin University. She was appointed as a full-time professor in the College of Electronics Science and Engineering, Jilin University in 2001. Her research interests are sensing functional materials, gas sensors, and humidity sensors.

Geyu Lu received the BS degree in electronic sciences in 1985 and the MS degree in 1988 from Jilin University in China and the Dr Eng degree in 1998 from Kyushu University in Japan. Now he is a professor of Jilin University, China. Now, he is interested in the development of functional materials and chemical sensors.